

Local Primordial Non-Gaussian Bias at the Field Level

James M. Sullivan,^{a,b,d,1,2} Shi-Fan Chen^c

^aDepartment of Astronomy, University of California, Berkeley, CA 94720, USA

^bBerkeley Center for Cosmological Physics, University of California, Berkeley, CA 94720, USA

^cInstitute for Advanced Study, 1 Einstein Drive, Princeton, NJ 08540, USA

^dCenter for Theoretical Physics, Massachusetts Institute of Technology, Cambridge, MA 02139, USA

E-mail: jms3@mit.edu, sfschen@ias.edu

Abstract. Local primordial non-Gaussianity (LPNG) couples long-wavelength cosmological fluctuations to the short-wavelength behavior of galaxies. This coupling is encoded in bias parameters including b_ϕ and $b_{\delta\phi}$ at linear and quadratic order in the large-scale biasing framework. We perform the first field-level measurement of b_ϕ and $b_{\delta\phi}$ using Lagrangian bias and non-linear displacements from N-body simulations. We compare our field level measurements with universality predictions and separate universe results, finding qualitative consistency, but disagreement in detail. We also quantify the information on f_{NL} available in the field given various assumptions on knowledge of b_ϕ at fixed initial conditions. We find that it is not possible to precisely constrain f_{NL} when marginalizing over $b_\phi f_{\text{NL}}$ even at the field level, observing a 2-3X degradation in constraints between a linear and quadratic biasing model on perturbative field-level mocks, suggesting that a b_ϕ prior is necessary to meaningfully constrain f_{NL} at the field level even in this idealized scenario. For simulated dark matter halos, the pure f_{NL} constraints from both linear and quadratic field-level models appear biased when marginalizing over bias parameters including b_ϕ and $b_{\delta\phi}$ due largely to the $f_{\text{NL}} b_\phi$ degeneracy. Our results are an important consistency test of the large-scale bias framework for LPNG and highlight the importance of physically motivated priors on LPNG bias parameters for future surveys.

¹Corresponding author.

²Brinson Prize Fellow

Contents

1	Introduction	1
2	Field Level Local Primordial Non-Gaussian Bias Model	2
2.1	LPNG bias	2
2.2	Field-level bias model	3
2.3	Numerical implementation	4
3	LPNG bias parameters	5
3.1	Universality at the field level	5
3.2	Field-level bias measurements at quadratic order	6
4	Field-level f_{NL} information	8
4.1	Perturbative mocks	10
4.2	Simulated halos	11
5	Conclusions	12
A	Simulation dependence	14
B	Renormalization of quadratic fields	15
C	Priors and profiles	16

1 Introduction

Cosmology links astronomically-observed large-scale fluctuations with high-energy physics in the early universe. Primordial non-Gaussianity (PNG) in the early universe imprints spatial correlations in the cosmic microwave background (CMB) fluctuations and large-scale structure (LSS), acting as a late-time window into inflationary physics [1, 2]. A particularly interesting variant is local PNG (LPNG) [3–7]: this type of PNG is forbidden for single-field inflation by a correlator consistency relation [8–10], and, as such, its detection would be a smoking gun for more exotic inflationary scenarios. The amplitude of local PNG, f_{NL} (here, we always mean $f_{\text{NL}} = f_{\text{NL}}^{\text{loc}}$), has been constrained by Planck data to be close to zero through a CMB bispectrum analysis at a level of $\sigma(f_{\text{NL}}) = 5.1$ [11, 12].

LSS observations, most immediately in the form of galaxy surveys, have the potential to exceed the statistical sensitivity of Planck on f_{NL} [13–32]. Unlike in the CMB, nonlinear dynamics and galaxy evolution preclude constraints on LPNG directly from the large-scale bispectrum of galaxies. In the language of perturbation theory, these nonlinearities manifest as free bias parameters which contribute to the bispectrum in a highly degenerate manner with the LPNG signal, thereby diluting the LPNG constraint (see e.g. refs. [33, 34] for the state-of-the-art in bispectrum LPNG constraints). On the other hand, LPNG also produces a very particular scale-dependent bias in the galaxy field that cannot be generated from Gaussian initial conditions and can be detected even at the level of the 2-point function (power spectrum) on very large scales [35–61]. This signal has an amplitude proportional to

the level of LPNG, f_{NL} , but is also proportional to an unknown coefficient b_ϕ , which depends on the small-scale astrophysics of the galaxy sample under consideration.

The scale-dependent bias due to LPNG allows us to constrain the amplitude $b_\phi f_{\text{NL}}$ instead of f_{NL} . To date, the majority of galaxy clustering data analyses have made strong assumptions about the value of b_ϕ to obtain tight constraints on f_{NL} [33, 34, 62–69], even when such assumptions may not be warranted for the observed tracers in question [41, 67, 70–72]. Given this state of affairs, it is natural to wonder if using observables beyond n -point functions can extract additional information about f_{NL} beyond the large-scale $b_\phi f_{\text{NL}}$ contribution in the presence of unknown galaxy nonlinearities¹. Many non- n -point statistics have been recently used to attempt to extract f_{NL} information without explicit priors on b_ϕ and some significant gains in f_{NL} information over e.g. the power spectrum, have been demonstrated in simulations [75–81]. However, these statistics often involve strong mixing of scales, or quantities that are not directly measurable, making their interpretation and use somewhat challenging.

Alternatively, it is possible to extract all the in-principle accessible information in the observed galaxy overdensity directly at the field-level, while still retaining perturbative modeling elements including scale-separation [82–91]. In this context, it is possible to explore questions of f_{NL} information (and the related question of b_ϕ priors) without regard to the information lost when compressing the field, e.g., into the galaxy power spectrum. Such exploration is the focus of this work. While it has recently been suggested based on analytic arguments that the available perturbative information at the field level is equivalent to that in n -point functions [92], other numerical investigations seemingly show large improvements from incorporating field-level information [84, 91], and it has also been suggested that the particular degeneracies of PNG with nonlinear dynamics can be broken in this way [93].

In this paper, we explore the feasibility of constraining f_{NL} using a field level forward model. For the first time, we use a bias model including extra operators generated by LPNG at the field level. We briefly review these operators, describe our field level bias model, and the N-body simulations used to compute galaxy trajectories and halo catalogs in Section 2. We present bias parameter measurements for simulated halos from a quadratic Lagrangian bias model, working at relatively large scales in Section 3 and quantify the in-principle-accessible f_{NL} information at the field level (at fixed phases) with this model using perturbative mocks in Section 4. We discuss the implications of these results in Section 5.

2 Field Level Local Primordial Non-Gaussian Bias Model

2.1 LPNG bias

Let us briefly review the LPNG bias signal in perturbation theory. Local PNG is a simple phenomenological model for the Bardeen potential $\phi(\mathbf{x})$ such that

$$\phi(\mathbf{x}) = \phi_G(\mathbf{x}) + f_{\text{NL}} (\phi_G^2(\mathbf{x}) - \langle \phi_G^2(\mathbf{x}) \rangle), \quad (2.1)$$

where ϕ_G is a Gaussian field². Non-zero f_{NL} in this model generates a modulation of short-scale physics by long-wavelength modes (e.g. generating a squeezed bispectrum, collapsed trispectrum, non-trivial position-dependent power spectrum, etc.). Through a simple peak-background split argument [37, 65], one can show that the local variance of scalar fluctuations

¹A parallel and more empirical strategy is to more precisely quantify the sizes of these nonlinearities through numerical simulations [73, 74], such that the effect of LPNG in the bispectrum can be carefully isolated.

²We neglect higher-order Local PNG, e.g. due to $g_{\text{NL}}, \tau_{\text{NL}}$. See, e.g., Refs. [55, 94] for discussion.

is rescaled by the presence of a long-wavelength mode. For a Fourier mode in the infinite-wavelength limit, $k \rightarrow 0$, this amounts to a rescaling of the amplitude of scalar fluctuations with finite wavelengths (i.e. A_s or σ_8). Since the number density of tracers (e.g. halos, galaxies) n_t is sensitive to the amplitude of these fluctuations this produces a scalar bias

$$b_\phi^{(\text{SU})} = 2 \frac{d \log n_t}{d \log \sigma_8} \quad (2.2)$$

which captures the response of tracer number density to a change in the amplitude of fluctuations. We term equation 2.2 the variance Separate Universe (SU) [95] version of LPNG bias to distinguish it from our field-level measurements. Assuming that the number density of tracers is a universal function of halo peak height [65]

$$b_\phi^{(\text{UMF})} = 2\delta_c b_\delta, \quad (2.3)$$

where b_δ is the linear Lagrangian bias, and $\delta_c = 1.686$ is the critical overdensity threshold for spherical collapse. This final approximation, or a slight modification of it, has frequently been used in the literature to model LPNG bias.

The above argument shows that, in the presence of LPNG, an extra term is needed in the bias expansion for tracer overdensity [37, 58]. At leading order, we have in the Eulerian bias expansion:

$$\delta_t(\mathbf{x}) = b_1 \delta(\mathbf{x}) + b_\phi f_{\text{NL}} \phi(\mathbf{x}) + \epsilon(\mathbf{x}), \quad (2.4)$$

where ϵ is a stochastic field. Terms involving $b_\phi f_{\text{NL}}$ then enter the n -point statistics of the tracer field. For example, the tracer power spectrum using only a linear (Gaussian) bias is augmented by a contribution that can be written as:

$$P_{tt}(k) = (b_1 + b_\phi f_{\text{NL}} \mathcal{M}^{-1}(k))^2 P_L(k) + \frac{1}{\bar{n}}, \quad (2.5)$$

where b_1 is the Eulerian linear bias, $P_L(k) = \langle \delta(\mathbf{k}) \delta(\mathbf{k}') \rangle'$ for the linear matter overdensity field δ , and $\mathcal{M}(k) = \frac{\delta(k)}{\phi(k)}$ is the normalized transfer function. The second term accounts for Poisson shot noise, which is typically subdominant on the linear scales on which this expression is good approximation.

2.2 Field-level bias model

In this work, we will go beyond linear bias by using a Lagrangian biasing model [96–99] and nonlinear displacements obtained from N-body simulations (see Section 2.3) as in Refs. [100–108]. In detail, this means the Lagrangian fields that constitute the biasing operators used to model $\delta_t(\mathbf{x})$ are connected to their Eulerian positions by “advection” via the non-linear displacements, and are denoted by $\mathcal{O}^{o,\text{adv}}(\mathbf{q})$. As described in Ref. [100], this is achieved by weighting the N-body matter tracer particles by the Lagrangian operators via gridded interpolation, and displacing them using the tracer particle locations at the final redshift of interest (see Section 2.3 for numerical details).

We employ a 2nd-order Lagrangian bias model for biased tracers at the field level

$$\begin{aligned} \delta_{t,\text{fwd}}^G(\mathbf{x}) &= \delta(\mathbf{x}) + b_\delta D(z) \delta^{\text{adv}}(\mathbf{q}) \\ &+ b_{\delta^2} D^2(z) \delta^{2,\text{adv}}(\mathbf{q}) + b_{K^2} D^2(z) K_{ij}^{2,\text{adv}}(\mathbf{q}) \\ &+ b_{\nabla^2 \delta} D(z) (\nabla^2 \delta)^{\text{adv}}(\mathbf{q}) \\ &+ \epsilon_t(\mathbf{x}), \end{aligned} \quad (2.6)$$

as well as its linear restriction, where $\delta(\mathbf{x})$ is the Eulerian matter density field, $D(z)$ is the linear scale-independent growth factor of matter fluctuations normalized to its $z = 0$ value, ϵ_t is the tracer stochasticity field, and we include operators up to second order in δ as well as at leading order in derivatives. We note that the superscript “ G ” indicates the usual “Gaussian” bias expansion, but, to be clear, all operators for $f_{\text{NL}} \neq 0$ cosmologies are generated using an overdensity $\delta = \mathcal{M}\phi$ where ϕ is the *non-Gaussian* field. Therefore these terms lead to, e.g., the leading primordial bispectrum contribution. We note that, while we will mostly be concerned with halos here, this language is fully general for other biased tracers like galaxies. The leading derivative correction partially absorbs numerical effects from the grid, due to both the finite resolution of the observed fields and missing dynamical contributions from short-wavelength modes, removing the leading-order resolution dependence of the model other than those already absorbed by the stochastic noise term ϵ_t . We neglect the quadratic stochasticity $[\epsilon_t\delta]$, and therefore the stochastic contributions to b_δ , though we note that including it would tend to decrease the amount of PNG information at the field level especially in the more realistic case that the phases of the initial conditions are unknown.³

The presence of LPNG introduces additional contributions to the bias expansion. To take these into account we augment the bias expansion by

$$\delta_{t,\text{fwd}}(\mathbf{x}) = \delta_{t,\text{fwd}}^G(\mathbf{x}) + b_\phi f_{\text{NL}}^{\text{loc}} \phi^{\text{adv}}(\mathbf{q}) + b_{\delta\phi} f_{\text{NL}}^{\text{loc}} D(z) [\phi\delta]^{\text{adv}}(\mathbf{q}), \quad (2.7)$$

where the quantity $[\phi\delta]^{\text{adv}}$ is computed prior to smoothing (and is *not* the product of the smoothed fields ϕ^{adv} and δ^{adv}). We keep the above expansion to first order in f_{NL} (see Ref. [33] for an estimate of the importance of these effects when measuring f_{NL} from the power spectrum). The leading higher-derivative correction to b_ϕ is approximately degenerate with b_δ , especially at large scales, so we will not fit it separately. As in the Gaussian case above we neglect the second-order stochastic fields that PNG induces [37].

Integrating over the stochastic field ϵ_t , we use a real-space likelihood [88, 101, 109]:

$$-2 \log(L(\delta_t(\mathbf{x}), \mathbf{p})) = \sum_{i=1}^{N_g^3} (2\pi\sigma_0^2) + \frac{(\delta_t(\mathbf{x}_i) - \delta_{t,\text{fwd}}(\mathbf{x}_i, \mathbf{p}))^2}{\sigma_0^2}, \quad (2.8)$$

where the free parameters of the theory model are $\mathbf{p} = \{f_{\text{NL}}, b_\delta, b_\phi, b_{\delta^2}, b_{K^2}, b_{\nabla^2\delta}, b_{\delta\phi}\}$ and we neglect the position-dependence of the noise ($\sigma_0^2 = P_{\epsilon_t}^0/V_{\text{cell}}, V_{\text{cell}} = (L/N_g)^3$). Since we assume the noise to be Gaussian, the inference of the biasing parameters reduces to simple linear regression with the best-fit bias parameters independent of σ_0 . We maximize the log likelihood to obtain bias parameters which implies that the best-fit σ_0 is given by the standard deviation of the residuals for the best-fit model.

2.3 Numerical implementation

We evolve the matter field from redshift $z_{\text{ini}} = 99$ to $z = 0$ using **FastPM** [110] in a box of size $L = 2000 \text{ Mpc}/h$, with $N_p = 1024^3$ simulation particles and force resolution “boost” factor of $B = 2$, using 40 timesteps. We compute the linear theory power spectrum used to generate

³The modification to the likelihood in Equation 2.8 including such density-dependent stochasticity was derived in Ref. [109]. Roughly, the noise σ_0^2 gains linear and quadratic dependencies on δ , i.e. $\sigma_0^2 \rightarrow \sigma^2(\delta) = \sigma_0^2 + \sigma_1^2\delta + \sigma_2^2\delta^2$. In the fixed initial conditions setup that we employ throughout this work, these additional free coefficients can be, in principle, solved for numerically, though the process will be slightly more involved than for a constant σ_0 due to the density dependence in $\sigma(\delta)$ up- and down-weighting over(under)dense regions.

initial conditions using `CAMB` [111], and use the Λ CDM parameters $\Omega_m = 0.3175$, $\Omega_b = 0.049$, $h = 0.6711$, $A_s = 1.91 \times 10^{-9}$ ($\sigma_8 = 0.834$) and $n_s = 0.9624$. We find halos using the `FastPM` implementation of Friends-of-Friends (FoF) with linking length $\ell = 0.2$. We consider a variety of halo mass bins, which are specified as necessary in subsequent sections. We use simulations with LPNG amplitudes of $f_{\text{NL}} = \{-100, -50, -25, -10, -5, -1, 0, 1, 5, 7, 10, 25, 50, 100\}$. We will work at redshift $z = 1$ unless otherwise stated.

Injecting local PNG into the Gaussian initial conditions $\phi_G(\mathbf{k})$ is possible via the numerical implementation of equation 2.1 using real Discrete Fourier Transforms (RFFTs)

$$\phi(\mathbf{x}) = \text{RFFT} [\phi_G(\mathbf{k}) + f_{\text{NL}} \text{RFFT}^{-1} [\text{RFFT}[\phi_G]^2(\mathbf{x}) - \langle \text{RFFT}[\phi_G]^2(\mathbf{x}) \rangle]] .$$

These local PNG initial conditions are implemented in the current publicly-available version of `FastPM` [110], where the initial field $\phi_G(\mathbf{k})$ is smoothed with a sharp- k filter beyond $k_s = \frac{1}{4}k_{\text{Nyq}}$ to suppress numerical artefacts due to aliasing in the quadratic local transformation. We additionally checked for artefacts due to squaring the field on the grid by confirming that doubling the resolution of the initial conditions has no significant impact on our results.

We follow a procedure similar to that of Ref. [100] to compute the advected fields using `nbodykit` [112]. We compute Lagrangian operator fields $\delta, \delta^2, K_{ij}^2, \nabla^2 \delta, \phi, \phi \delta$ from the linear matter overdensity field at the same resolution Λ as the initial conditions. We use LPNG-renormalized, or normal-ordered, quadratic Gaussian bias operators (see Appendix B for further details). We deposit these fields to particles and match the particle IDs to those at their final (Eulerian) location at $z = 1.0$ to advect the operators. We then paint the advected particles according to their Lagrangian field weight to obtain the fields on grids of various resolutions N_g^3 to obtain the components of the real-space likelihood in Equation 2.8. We will often also refer to the grid (Nyquist) wavenumber Λ associated with a particular resolution N_g . We compensate the linear mesh following Ref. [113]. When using linear regression to obtain the bias parameters or when estimating f_{NL} in our profile likelihood procedure, we will always fit in real space using all modes on the grid with cell-size $\Delta = L/N_g$ (i.e., roughly, $r_{\text{min}} \approx \Delta$, or $k_{\text{max}} \approx \Lambda$; see Appendix B for further discussion).

3 LPNG bias parameters

In this section we present the results of our field-level bias measurements, including the LPNG bias parameter b_ϕ as a function of the linear bias along with other bias parameters in the quadratic model. We discuss the implications for the field level information content with respect to f_{NL} in the next section.

3.1 Universality at the field level

Figure 3.1 shows the measured values of b_ϕ and $b_1^L = b_\delta$ using the field-level model with Gaussian errorbars and linear regression for six mass bins that are equally spaced in log halo mass $\log\left(\frac{M_h}{M_\odot/h}\right)$. The results here were obtained using a linear bias model varying only b_δ, b_ϕ , but using a quadratic model yields quantitatively similar results. The squares show the variance separate universe predictions for b_ϕ plotted against b_1^L values that are obtained by fits to power spectra. In detail, we obtain the linear bias (used for the SU points in Figure 3.1) as the large-scale ratio of the halo-matter cross power spectrum $P_{hm}(k)$ to the matter power spectrum $P_{mm}(k)$ up to $k_{\text{max}} = 0.05 h/\text{Mpc}$. For the values of the variance SU bias, we measure $b_\phi^{(\text{SU})}$ using the version of eqn. 2.2 as in Ref. [71] (centered finite difference

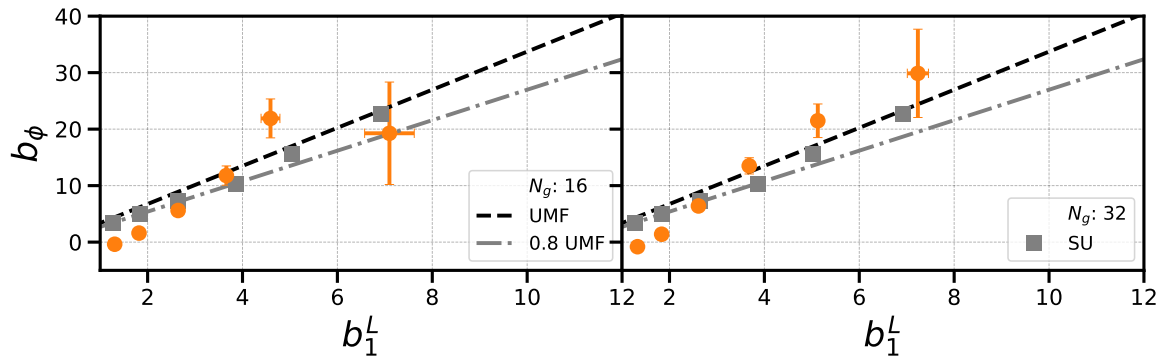


Figure 1. *Linear/PNG bias* The $b_\phi(b_1^L)$ measurements from field level fits for two (small) choices of cutoff wavenumber Λ , corresponding to the grid scale with $N_g = \{16, 32\}$ 1-dimensional cells in the left and right panels, respectively. The bias values measured with the field-level model (and their associated uncertainties) are shown in orange. The separate universe measurements are plotted as gray squares, and the universality relation is plotted in black dashed, with its empirical modification (by a factor of 0.8) plotted in gray dashed.

in relative amplitude change $\delta\sigma_8$) at $\sigma_8 = 0.834(1 \pm \delta\sigma_8)$, with $\delta\sigma_8 = 0.02$. Using a step in σ_8 twice or half as wide has sub-percent impact on the estimated bias values.

The black dashed line shows the universal mass function (UMF) prediction $b_\phi^{(UMF)} = 2\delta_c b_\delta$ of eqn. 2.3. The gray dash-dotted line shows $b_\phi = 0.8 \times 2\delta_c b_\delta$, which has been shown to provide a better fit to dark matter halos in simulations [71]. Overall, we see that the field-level fits qualitatively agree with the UMF and SU predictions within the errorbars for large values of the bias. However, at small values of the linear bias (small halo masses) we see some multi- σ disagreement - we have verified this is not due to several aspects of our simulation resolution or the approximate nature of FastPM - see Appendix A for further discussion.

3.2 Field-level bias measurements at quadratic order

Figure 2 shows field-level constraints on the quadratic and LPNG Lagrangian bias parameters when including the nonlinear bias terms in Equations 2.6 and 2.7. These Gaussian contours are obtained through simple linear regression using the field-level likelihood in eqn. 2.8, which is equivalent to considering all real-space 2-point functions of the linear and quadratic operators. We obtain nearly identical results—up to differences in scale cuts—working in Fourier space. The data vector consists of a mass-binned N -body halo density field obtained from a simulation with $f_{\text{NL}} = 100$. The likelihood noise σ_0 is set to its optimal value (estimated from the residuals in eqn. 3.1) and no priors are placed on the bias parameters. We note that to obtain sensible constraints from this quadratic bias model, it is crucial to use the renormalized quadratic Gaussian component fields (δ^2, K^2) as part of the regression basis, a point we discuss further in Appendix B.

The constraints on the linear LPNG bias, in the combination $b_\phi f_{\text{NL}}$, are shown in the second column. Considering first the 1D posterior at the top, it is apparent that the constraining power on $b_\phi f_{\text{NL}}$ does *not* change much with the likelihood cutoff scale Λ . On the other hand, the constraints on the Gaussian bias parameters in Equation 2.6 noticeably improve as Λ increases. This is as expected, since the information on $b_\phi f_{\text{NL}}$ (at fixed f_{NL}) is coming from large scales. Importantly, we do not see much correlation between the linear LPNG bias with

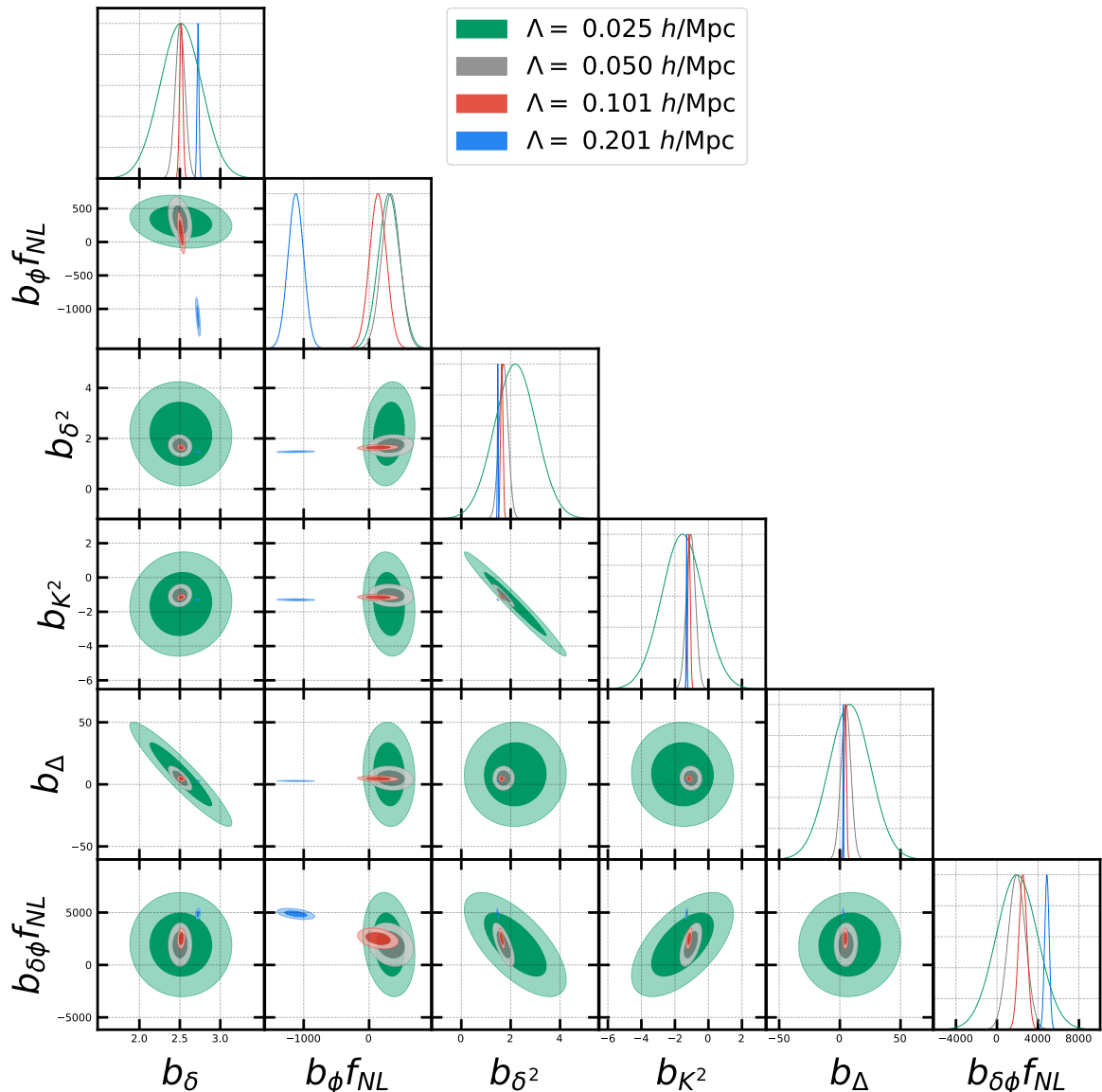


Figure 2. *Quadratic/PNG bias values:* Constraints on quadratic Local PNG bias parameters obtained from linear regression at several grid smoothing scales Λ (colors) for a mass bin, $\log_{10} \left(\frac{M_h}{M_\odot/h} \right) = [13.62, 13.71]$.

the other bias parameters, while all the quadratic bias parameters show nontrivial degrees of correlation, including the LPNG one $b_{\delta\phi} f_{NL}^{\text{loc}}$.

The fact that the contours are nested within each other at the $1\text{-}\sigma$ level for all scales Λ up until the maximum value of $\Lambda = 0.2 h/\text{Mpc}$ indicates that the model is consistently fitting the bias parameters across scales (i.e. there is very limited “running” of the bias parameters with Λ). The exception to this statement is the $\Lambda = 0.2 h/\text{Mpc}$ (blue) contour, where a systematic bias is produced⁴, which we now discuss.

⁴We verified that this bias at maximum Λ is reproduced in fits to Gaussian simulations as well, indicating the bias is not due to the inclusion of PNG bias.

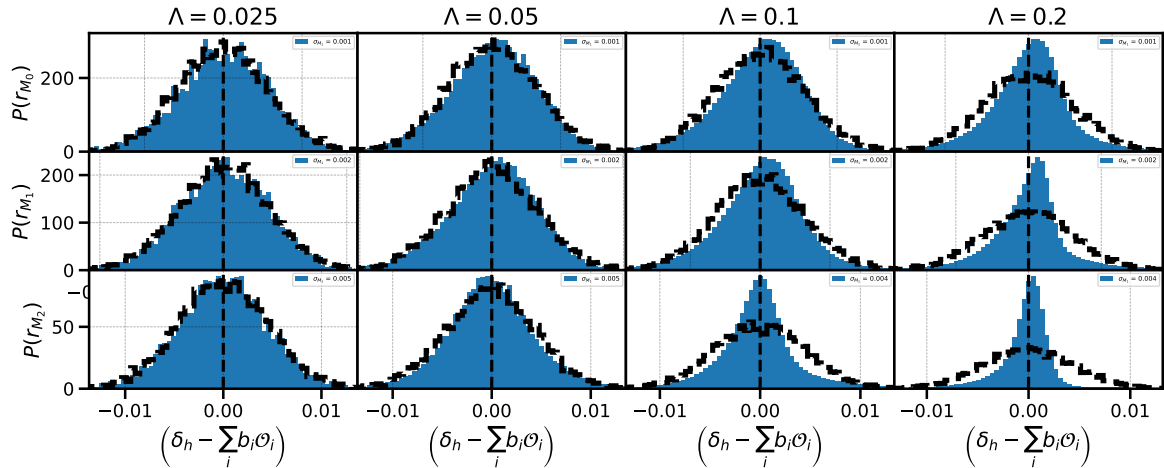


Figure 3. *Residual PDFs:* Residual probability density functions for several choices of halo mass and smoothing scale using the quadratic biasing model. The three halo mass bins shown have bin edges $\log_{10} \left(\frac{M_h}{M_\odot/h} \right) = \{13.1, 13.5, 14.0, 14.5\}$, and increase with increasing row number, while the grid cutoff scale (Λ , in h/Mpc) used for the fields increases with increasing column number. For visual clarity, the residuals are normalized by the number of grid volume elements, N_g^3 .

To assess the reason for the large bias at the largest value of Λ , we can consider the probability density function (PDF) of the field-level residuals entering the likelihood

$$r_M(\mathbf{x}) = \delta_{h,M}(\mathbf{x}) - \delta(\mathbf{x}) - \sum_i b_i^M \mathcal{O}^{(i)}(\mathbf{x}). \quad (3.1)$$

Figure 3 shows this PDF for all halo mass bins with variation in smoothing scale and f_{NL} value. The empirical scatter σ_0 is quoted in the legend for each PDF. As expected, going to higher halo masses (down the column) produces increased values of σ_0 , as there are fewer high-mass halos. Similarly, we see that going to higher values of the cutoff Λ results in more non-Gaussian densities - this behavior has been seen previously for field-level bias modeling (see e.g. Table III of Ref. [82]). Already some non-Gaussianity in the PDF is developing for the most massive halos at $\Lambda = 0.1 h/\text{Mpc}$, though this appears not to affect the bias parameter constraints obtained from the likelihood fits in Fig. 2. Clearly at the largest value of Λ (corresponding to $N_g = 128$) our Gaussian field-level likelihood breaks down significantly, and we do not expect it to produce unbiased constraints on $b_\phi f_{\text{NL}}$, and we will see that this is indeed the case in Section 4.2.

4 Field-level f_{NL} information

To test the potential to constrain f_{NL} at the field level, we infer f_{NL} by way of a profile likelihood procedure. Rather than attempt to marginalize over initial conditions, we work with fixed initial conditions. This provides a clear picture of the constraining power of the field level model in an idealized case, providing an upper bound on the information content of the field using our model. These results, of course, should not be interpreted as reflecting what uncertainty on f_{NL} is actually achievable for real LSS tracers, but rather are meant to quantify the information on f_{NL} that is available at the field level in different scenarios when

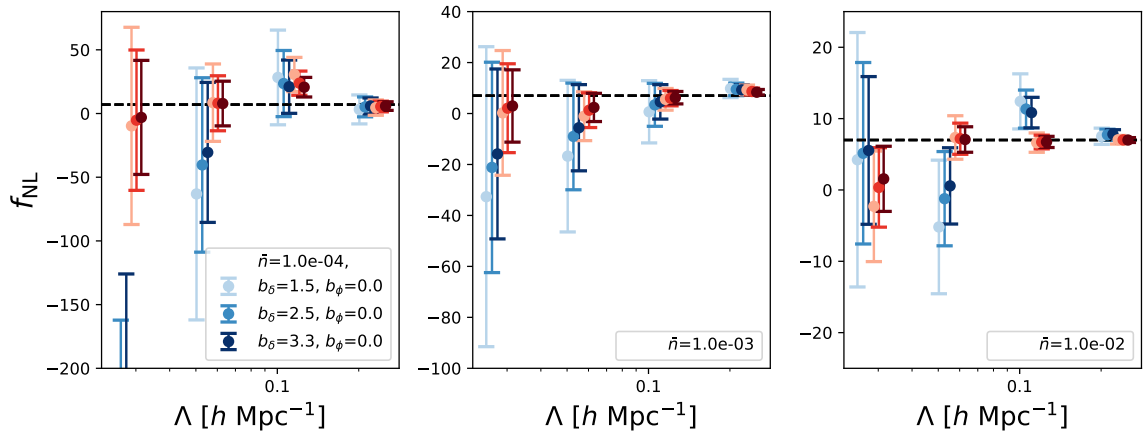


Figure 4. *Zero quadratic/PNG bias:* Field-level constraints on f_{NL} obtained from perturbative mocks. Values of f_{NL} , $\sigma(f_{\text{NL}})$ are obtained from fitting the profile likelihood curvature and are shown as a function of the cutoff scale Λ . The true value of $f_{\text{NL}} = 7$ used to generate the mock is marked by the dashed black line. Red and blue colors correspond to constraints obtained from the linear and quadratic cases. Different shades of a single color correspond to different input linear biases for the mocks. Each panel corresponds to a different level of Poisson noise injected into the mock. Constraints from mocks with distinct bias values have been horizontally offset for clarity. (We draw the reader’s attention to the changing vertical axis in each panel.)

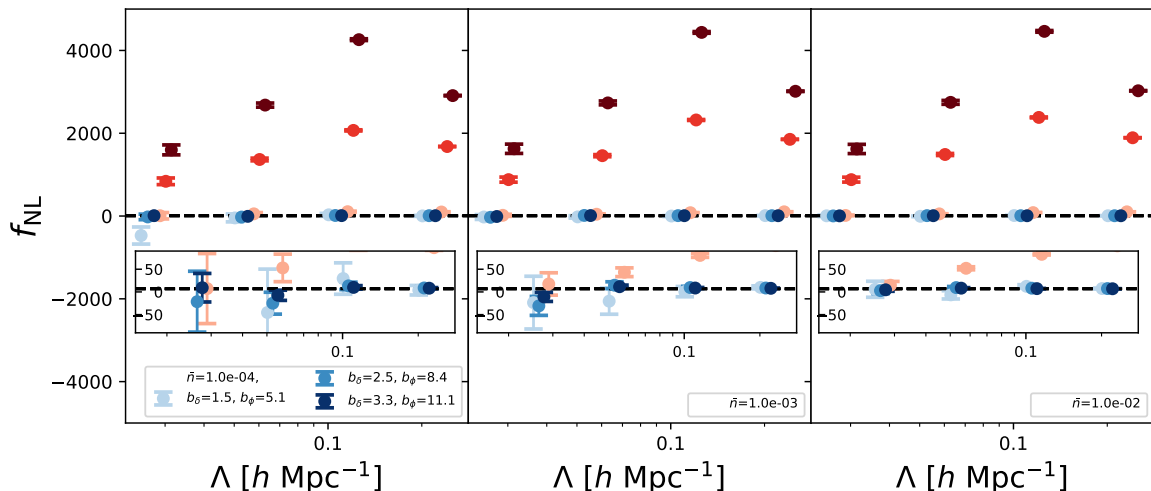


Figure 5. *Non-zero quadratic/PNG bias:* Similar to Figure 4, but for nonzero values of the quadratic and PNG bias parameters. The inset shows a significant zoom-in of the y-axis, and reveals the unbiasedness of the quadratic model (blue points) relative to the linear model (red points).

marginalizing over bias parameters. In practice, the initial conditions must be marginalized over in order to constrain f_{NL} in a full field-level inference framework - a task that is an area of vigorous ongoing research [84, 114–129]. We consider the case of both perturbative mocks (generated by adding noise to our bias model) and simulated dark matter halos in this Section.

4.1 Perturbative mocks

We perform two tests of f_{NL} information contained in the field using perturbative mock tracers generated from our bias model. Figures 4 and 5 show constraints from a field-level profile likelihood procedure, similar to that used by Ref. [88] to constrain σ_8 from simulated halos at fixed initial conditions⁵. We set as our data a perturbative mock with a value of $f_{\text{NL}} = 7$, and compute the maximum likelihood value of f_{NL} for each of our f_{NL} simulations, marginalizing over the bias parameters and fitting for σ_0 . By fitting a parabola to the log likelihood, we obtain the central value and $\pm 1\sigma$ uncertainties on f_{NL} . The bias parameters are implicitly marginalized over with uniform priors during linear regression (see Appendix C for other choices of prior). We perform this procedure for several smoothing scales $\Lambda = \{0.025, 0.05, 0.1, 0.2\}h/\text{Mpc}$ (horizontal axis). Each panel of Fig. 4 and Fig. 5 shows the constrained value of f_{NL} from the profile likelihood procedure applied to a mock generated from the quadratic biasing model with a different level of injected Poisson noise, corresponding to number densities of $\bar{n} = \{10^{-4}, 10^{-3}, 10^{-2}\} [h/\text{Mpc}]^3$. We use mock linear bias parameters of $b_\delta = \{1.5, 2.5, 3.3\}$, which are represented by different color shades. The red points show results for f_{NL} using a linear model and the blue points for using a quadratic model. The lightest (darkest) shade of red and lightest (darkest) shade of blue correspond to a mock with the same linear bias value fitted by the linear model and quadratic model, respectively.

In Figure 4 we set all bias parameters to zero except for b_δ , including the PNG bias coefficients. This test therefore probes the impact of simply varying the quadratic bias parameters rather than fixing them on the f_{NL} information contained in the density field at the field level. In each panel, we see that increasing the cutoff scale Λ results in increasingly tight constraints on f_{NL} when marginalizing over bias parameters. This indicates that we are accessing nonlinear information contained in the density field. However, when comparing the linear (red) and quadratic (blue) mock and model results, we see that in each panel, for any choice of mock bias parameters (same shade) or cutoff scale Λ , the errorbars increase by a factor of more than 2-3. The non-linear information being probed is apparently obscured by the lack of knowledge of the quadratic bias parameters. This is consistent with existing results in the literature [33, 67], which suggest that, at least for volumes of existing survey data, the primordial contribution to the tracer bispectrum does not lead to improved constraints on f_{NL} in practice. In fact, here we can make an even stronger statement about the low impact of this term on f_{NL} information since we work at the field level and at fixed phases.

In Figure 5 we set bias parameters to those fitted to halos (as a function of b_δ) in the literature. Specifically, b_ϕ is set with the universality relation (eqn. 2.3), b_{δ^2} and b_{K^2} are set using the (Gaussian) measurements of Ref. [98], $b_{\nabla^2\delta}$ is fixed to zero, and $b_{\delta\phi}$ is fixed to its universality prediction⁶. As expected, in each panel at fixed number density, the larger the true value of b_ϕ , the larger the $b_\phi f_{\text{NL}}$ signal at fixed f_{NL} , resulting in tighter constraints on f_{NL} ⁷. While in Fig 4 the linear model could accurately fit the quadratic mock, here obviously this will not be the case. However, it is quite striking that even on very large scales (low Λ) we see that the linear model (red points) generally returns extremely biased results when attempting to fit to a quadratic perturbative mock. This is an indication

⁵We are able to approximately reproduce the results of Ref. [88] with our procedure, e.g. in their Fig. 3, though the results are not directly comparable due to differing forward models.

⁶E.g. as stated in Ref. [130] eqn. 1.5.

⁷We also note that the amount of injected noise, which is separate from the bias value used to generate the mock in this context (as opposed to the case of halos/realistic tracers), generally appears not to bias the inferred value of f_{NL} .

that even on very large scales, it is not possible to constrain f_{NL} for a nonlinear tracer like halos and galaxies without also marginalizing over quadratic bias parameters, i.e. significant degeneracies exist between higher-order bias parameters and f_{NL} even at the field level when b_ϕ is free. Heuristically, without knowing the value of b_ϕ , the leading signal for f_{NL} comes from primordial contributions to the bispectrum; however, since the leading contributions to the bispectrum are gravitational and depend on the values of b_{δ^2}, b_{K^2} , fixing the values of the nonlinear bias parameters leads to a misattribution of the primordial signal and thus biased f_{NL} constraints even for small Λ .

4.2 Simulated halos

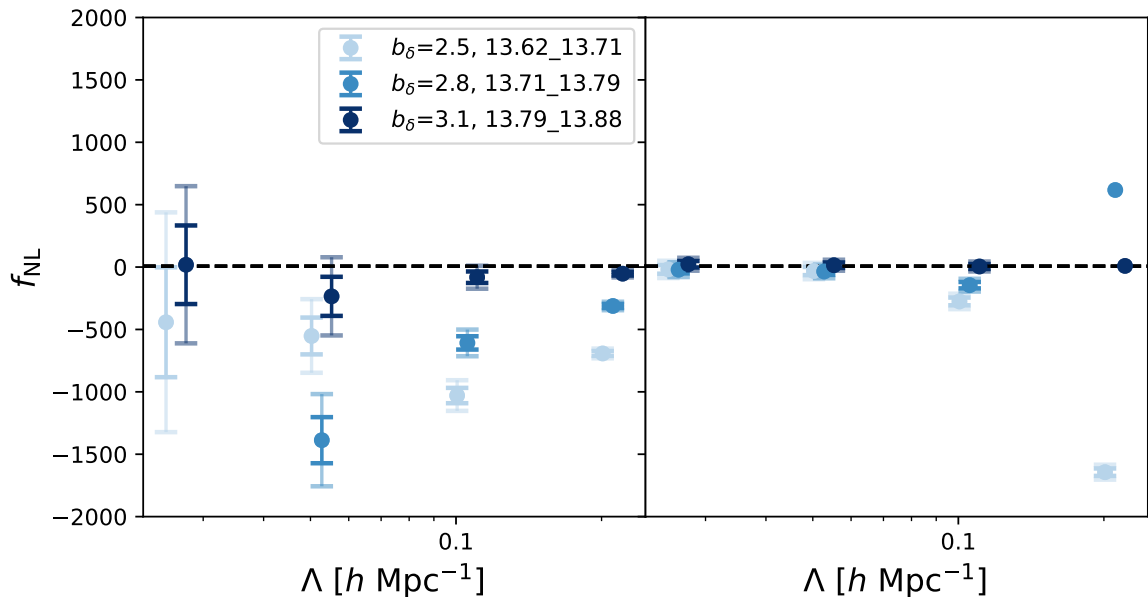


Figure 6. *Quadratic + halos:* Field-level constraints on f_{NL} obtained from N-body halos using a quadratic biasing model (at 1- σ and 2- σ). As in Figs. 4, 5, constraints are obtained from our profile likelihood procedure. The true value of $f_{\text{NL}} = 7$ used to run the simulation is marked by the dashed black line. *Left:* Constraints from halos when marginalizing over all bias parameters. It is clear that results are biased, especially for certain halo mass bins. *Right:* The same profile likelihood procedure, but where all values of the PNG biases $b_\phi, b_{\delta\phi}$ are fixed to their best-fit values for *each* f_{NL} , thus breaking the $b_\phi f_{\text{NL}}$ degeneracy. We see that in this case, constraints are unbiased for the halo sample in question for all but the highest Λ .

Figure 6 shows profile likelihood f_{NL} constraints obtained from N-body halos with a quadratic biasing model. In general, we find in the left panel that constraints on halos are significantly biased, though there are some mass bins for which this is not the case. This is due to the $b_\phi f_{\text{NL}}$ degeneracy⁸: the right panel of Fig. 6 shows what happens when we perform the profile likelihood procedure with PNG bias parameters fixed to their best fit values for each f_{NL} simulation⁹, which completely breaks this degeneracy. Except for the highest Λ , for which we showed the quadratic bias model is insufficiently accurate in Section 3.2, the constraints

⁸We thank Fabian Schmidt for productive discussions around this point.

⁹We note that for the smaller values of f_{NL} , the value of b_ϕ is not well constrained. The results are therefore most sensitive to the fitted values of the simulations with larger f_{NL} .

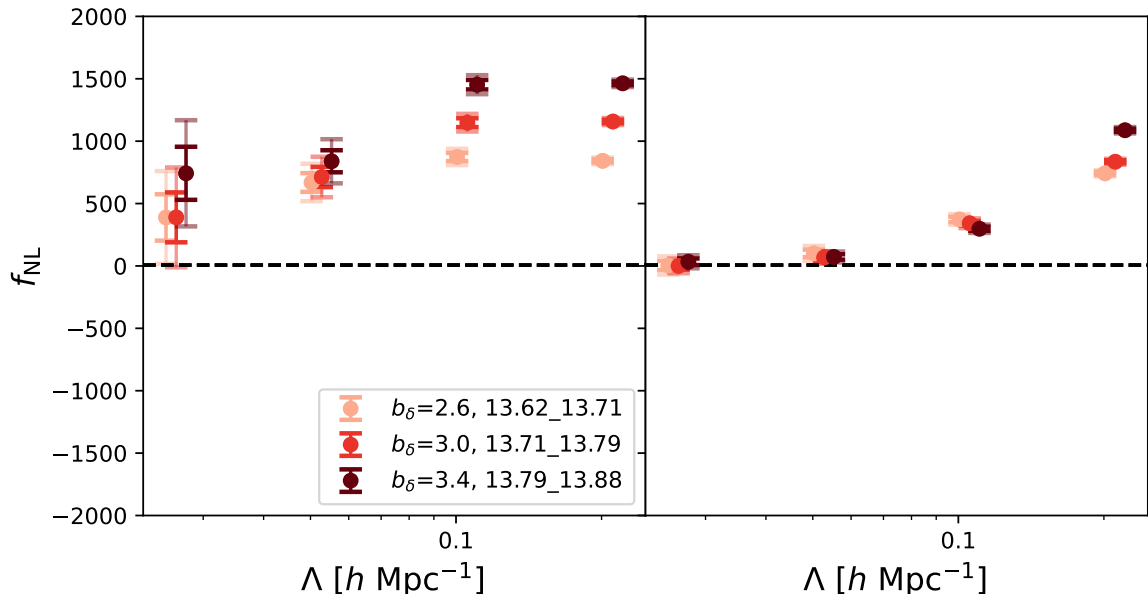


Figure 7. *Linear + halos:* Similar to Figure 6, but using a linear bias model. By comparison, the results are generally significantly more biased (with smaller error bars), even on large scales, and are biased toward high f_{NL} , while the opposite is true for the quadratic model in Fig. 6. The right panel also shows the expected failure of the linear bias model when the PNG biases are fixed for all but the lowest values of Λ .

are unbiased. While for the mock test we showed that there is significant f_{NL} information in the nonlinear density field (Figs. 4,5), for N-body halos it appears that constraints obtained from fitting a quadratic model are biased due to the $b_\phi f_{\text{NL}}$ degeneracy. This suggests that marginalizing over the PNG bias parameters, and hence the large-scale local PNG bias signal, is not a feasible strategy for constraining f_{NL} at the field level from halos. In short, unbiased constraints of f_{NL} from tracers at least as complicated as simulated halos using a quadratic bias model are only attainable with prior knowledge on b_ϕ and $b_{\delta\phi}$. Figure 7 shows that the difficulty is even more pronounced in the case of a linear bias model, and persists even at the lowest Λ where the linear model should be accurate. The errorbars on the halo constraints are relatively large compared to the mocks due to the narrow mass bins we consider for these simulations - it would be interesting to extend these results with larger volume simulations and higher number densities.

5 Conclusions

Local primordial non-Gaussianity (LPNG) is a signal of the inflationary era that can be probed with large-scale structure surveys. Given recent technological and methodological developments, performing field-level inference of cosmological parameters using the galaxy distribution is becoming increasingly feasible. In this paper, we use a field-level Lagrangian biasing model to perform the simple extension of existing perturbative field-level models to the case of LPNG at quadratic order while using fully non-linear displacements. We use this machinery to test the widely-used universality relation between the LPNG bias b_ϕ and the linear (Eulerian) bias $b_1 = 1 + b_\delta$ for simulated dark matter halos, finding rough agreement with

results from variance separate-universe simulations. We also obtain constraints on quadratic bias parameters, including LPNG parameters b_ϕ , $b_{\delta\phi}$ of simulated halos at the field level using several smoothing scales Λ , finding that the results from our biasing model are stable below wavenumbers of $\Lambda = 0.2 h/\text{Mpc}$ at $z = 1$. Finally, we use perturbative mocks, simulated dark matter halos, and a field-level profile likelihood to obtain constraints on f_{NL} while marginalizing over all bias parameters, including LPNG bias parameters—we find that using a quadratic bias model, as is necessary for all but the largest scales probed by cosmological observations, degrades the constraints on f_{NL} by a factor of greater than 2-3. We also find that constraints on f_{NL} from halos are generally quite biased, even with the quadratic model, due to the $b_\phi f_{\text{NL}}$ degeneracy. We can make several conclusions based on these results.

Our simple test of the f_{NL} information available at the field level when marginalizing over nonlinear bias has implications for recent efforts toward field-level inference of cosmological parameters, including f_{NL} . We show that there *is* information that can be captured from the field level with our bias model when marginalizing over all bias parameters. Naively, this would suggest that we are able to extract significant nonlinear information from the tracer density field, which is in agreement with, e.g. Refs. [56, 131–133], as we also found that constraints on the combination $b_\phi f_{\text{NL}}$ (at fixed f_{NL}) are essentially unaffected by changes in Λ , so any additional information must come from the matter density field itself. However, we also show that using a quadratic bias model (as necessary for using quasi-linear scales), degrades these constraints by a factor of a few - indicating that the nonlinear information is significantly diluted by their degeneracy with quadratic bias parameters. Furthermore, we found that the inference of f_{NL} from perturbative mocks generated using realistic values of quadratic halo bias parameters (including PNG bias parameters) is significantly biased when using a linear biasing model, showing that f_{NL} at the field level requires careful marginalization of nonlinear bias even at the largest scales. Finally, we showed that the inference of f_{NL} from simulated N-body halos when marginalizing over bias parameters (including PNG bias parameters) is in general quite biased due to the $b_\phi f_{\text{NL}}$ degeneracy. This suggests that trustworthy priors on PNG bias parameters will be essential for future constraints of f_{NL} from data using the scale-dependent bias signal.

The tests performed here on simulated dark matter halos, while far from observations, are the first use of the field-level bias model with LPNG to model the bias b_ϕ . This step is mechanically simple but will be a necessary piece of any future perturbative field-level inference of f_{NL} from tracers of large-scale structure. An obvious extension would be to further develop our LPNG extensions of the field-level biasing framework to redshift space [83, 89, 134]. Another application would be to measure LPNG bias from expensive hydrodynamical simulations where it is infeasible to run multiple cosmologies required for separate universe bias estimates. This is especially of interest if it is possible to link simulated tracers (galaxies, QSOs, line intensity, etc.) and particular target samples of a redshift survey. It would also be interesting to extend this work to field-level biasing models of non-local types of PNG.

Our results indicate that constraints on LPNG from large-scale structure will depend on informative b_ϕ priors. Such priors may be accessible from simulations e.g. through simulation-based priors [73, 74, 135, 136], internal consistency relations such as the $b_2(b_1)$ relation, suitably extended beyond the case of dark matter halos, or alternative methods of estimating b_ϕ . Here we operate at fixed phases, which is optimistic for higher order correlations, but multi-tracer analyses can remove the random effects of phases by canceling cosmic variance in n -point statistics where the LPNG bias contribution dominates [15, 18, 20, 22, 23, 30, 137, 138]. While there is significant f_{NL} information in the nonlinear density field, it seems likely

that constraints from large-scale structure will continue to be driven by the large-scale bias contribution.

Acknowledgments

We thank Kazuyuki Akitsu, Martin White, Matias Zaldarriaga, and especially Fabian Schmidt for useful discussions of field-level bias modeling, as well as Uroš Seljak and Simone Ferraro for helpful conversations and Biwei Dai for pointing out a bug in FastPM on NERSC’s Perlmutter. JMS also thanks members of the Quijote PNG group for discussions.

JMS was partially supported by the U.S. Department of Energy, Office of Science, Office of Advanced Scientific Computing Research, Department of Energy Computational Science Graduate Fellowship under Award Number DE-SC0019323 as well as a U.S. Dept. of Energy SCGSR award during the completion of this work. JMS also acknowledges that, in part, support for this work was provided by The Brinson Foundation through a Brinson Prize Fellowship grant. SC acknowledges the support of the National Science Foundation at the Institute for Advanced Study through NSF/PHY 2207583.

This research used resources of the National Energy Research Scientific Computing Center (NERSC), a Department of Energy Office of Science User Facility using NERSC award HEP-ERCAP0028635. This research has made use of NASA’s Astrophysics Data System.

A Simulation dependence

To test the extent to which our results depend on the resolution of the **FastPM** simulations used to advect the Lagrangian operators to their final positions, we test several force resolutions in FastPM. Figure 8 shows histograms for three redshift bins (those shown in Fig. 3) where each color corresponds to a different B corresponds to a different force resolution¹⁰. Here we see that the $B = 1$ case is significantly different from $B = 2$ and $B = 3$, the latter two of which agree well. We use $B = 2$ simulations in the main text.

As a further test, we measured the Lagrangian and LPNG bias parameters with displacements from **Gadget** [139]. Specifically, we used the Quijote-PNG [131] simulation suite (initial conditions, as well as dark matter particle snapshots and FoF halo catalogs at redshift $z = 1$) with $f_{\text{NL}} = 100$ ¹¹. These simulations were run with a lower particle resolution (512^3) and in a smaller box ($1 h^{-1}$ Gpc) than we use in the main text, but employ a tree solver for the small-scale particle-particle interactions, which are not captured by **FastPM**. We also use the renormalization procedure described in Section B for the Quijote-PNG field-level bias measurements, using the publicly available ICs. This comparison is performed at the same choice of Λ CDM cosmological parameters, and the Quijote-PNG bias parameters are shown in Figure 9. There we see that the $b_\phi(b_1)$ relation measured from Quijote-PNG is again qualitatively similar to the SU values (albeit with larger uncertainties), but in detail, the field level values disagree. This disagreement between field-level bias values and SU values (as well as the UMF relation) is much larger for Quijote-PNG than for our FastPM measurements. We speculate that the lower mass halos in both simulations may be affected low mass resolution, and note that doubling the IC particle grid for FastPM leads to changes in inferred b_ϕ for lower masses (though these changes are smaller than the disagreement with the Quijote points).

¹⁰The “boost” factor, B , is defined as the ratio of the force grid to the initial conditions grid [110].

¹¹Since Quijote-PNG only contains cosmologies with $f_{\text{NL}} = \pm 100$ we cannot reproduce the **FastPM** calcula-

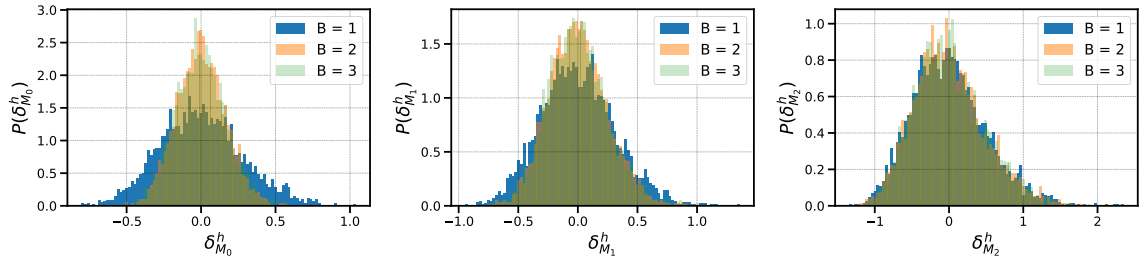


Figure 8. Histograms of the halo density field for several choices of force resolution in FastPM with $f_{\text{NL}} = 100$. There is a significant difference between the $B = 1$ and $B = 2$ cases, but not between $B = 2$ and $B = 3$.

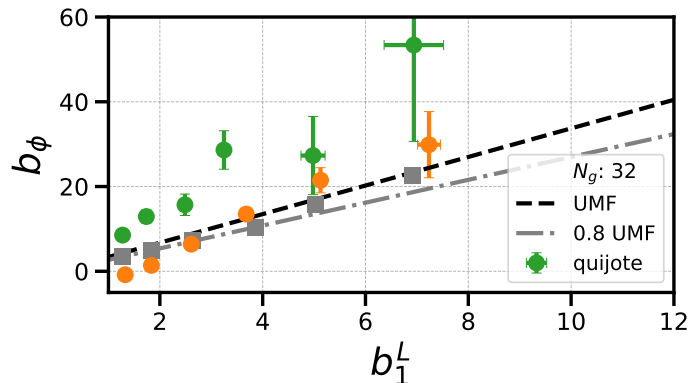


Figure 9. Similar to Figure 3.1, but with bias parameters measured for multiple FastPM as well as the Quijote-PNG simulations (green). The bias measurements for Quijote are consistent with those of FastPM at high values of b_1 $\Lambda \approx 0.05 h/\text{Mpc}$, but for low values of b_1 , the field-level fits to Quijote are significantly larger than the FastPM values and UMF predictions. In this comparison, the points plotted for the smaller Quijote box are using a grid with the same physical scale, but a grid resolution that is reduced by a factor of 2 (i.e. for Quijote $N_g^{(\text{Quijote})} = 16$).

B Renormalization of quadratic fields

We renormalize the quadratic operator fields $\delta_{\Lambda'}^2$, and $K_{\Lambda'}^2$, to remove the large-scale cutoff-dependent contributions introduced by LPNG [37, 38]

$$[\delta^2](\mathbf{k}) = (\delta_{\Lambda'}^2)(\mathbf{k}) - 4f_{\text{NL}}^{(\text{loc})} \sigma^2(\Lambda') \phi(\mathbf{k}), \quad (\text{B.1})$$

$$[K^2](\mathbf{k}) = (K_{\Lambda'}^2)(\mathbf{k}) - \frac{8}{3} f_{\text{NL}}^{(\text{loc})} \sigma^2(\Lambda') \phi(\mathbf{k}), \quad (\text{B.2})$$

where $\sigma^2(\Lambda') = \int_{\mathbf{k}} P_{\delta\delta}(k) W_{\Lambda'}^2(\mathbf{k})$. Failing to account for the renormalization of these terms produces numerically large large-scale contributions to the quadratic operators, which significantly influences the quadratic bias measurements. We perform the necessary renormalization subtraction in Lagrangian space using a slightly modified version of eqn. B.2 on the initial conditions grid before advecting the fields (therefore the Λ' in eqn. B.2 should be considered distinct from the Λ associated with N_g in the rest of this work).

tion quantifying the information on f_{NL} performed in Section 4.

While the fields involved are all computed on the initial conditions grid, the relation of eqn. B.2 was derived under the assumption of a spherically symmetric window $W_{\Lambda'}(k)$ [140] to perform the angular part of the bispectrum integral (see their Appendix C). As a result, if we take eqn. B.2 at face value, and associate $\sigma^2(\Lambda')$ with the variance of δ on the IC grid, we do not obtain the value of σ^2 in eqn. B.2 that removes large-scale cutoff dependence.

One can compute $\sigma(\Lambda')$ without the edge modes beyond Λ' that exist on the grid by removing these modes individually. It would also be possible to use a spherically symmetric filter for this purpose, but a sharp filter in k -space introduces artefacts in real space that would impact our field-level bias measurements. To test whether $\sigma^2(\Lambda')$ on the grid was being affected only by the numerics of edge modes, we massively suppressed with a hyperbolic tangent filter with smoothing scale $R = 50 \text{ Mpc}/h$ and compared the variance on this grid with the theoretical expectation from linear theory for σ^2 . We found that these values agreed to 4 significant figures, indicating that the small-scale modes indeed contributed to a change in $\sigma^2(\Lambda')$.

Rather than apply a filter to the grid, we empirically fit two free coefficients $\alpha = (\alpha_{\delta^2}, \alpha_{K^2})$ multiplying the component spectra to jointly minimize the large-scale pieces of the non-Gaussian component spectra. Specifically, the values of $\alpha = (\alpha_{\delta^2}, \alpha_{K^2})$ are fitted using Broyden-Fletcher-Goldfarb-Shanno (BFGS) algorithm [141, 142] ℓ_2 loss normalized by the diagonal Gaussian errors given by the Gaussian component power spectra

$$\alpha_{\delta^2}^* = \operatorname{argmin}_{\alpha_{\delta^2}} \sum_{k_i=k_f}^{k_{\max}=0.03 \text{ h/Mpc}} \frac{1}{\sigma_{\text{disc.},\delta^2}^2} \left(\langle \delta^2 \delta \rangle_G(k_i) - \langle \delta^2 \delta \rangle(k_i) + 4\alpha_{\delta^2} f_{\text{NL}} \sigma^2(\Lambda) \langle \phi \delta \rangle(k_i) \right)^2 \quad (\text{B.3})$$

$$\alpha_{K^2}^* = \operatorname{argmin}_{\alpha_{K^2}} \sum_{k_i=k_f}^{k_{\max}=0.03 \text{ h/Mpc}} \frac{1}{\sigma_{\text{disc.},K^2}^2} \left(\langle K^2 \delta \rangle_G(k_i) - \langle K^2 \delta \rangle(k_i) + \frac{8}{3} \alpha_{K^2} f_{\text{NL}} \sigma^2(\Lambda) \langle \phi \delta \rangle(k_i) \right)^2, \quad (\text{B.4})$$

where $\sigma_{\text{disc.},\delta^2}^2, \sigma_{\text{disc.},K^2}^2$ are the disconnected covariances for the spectra being fitted. This process, for example, gives $\alpha_{\delta^2} = 0.1$ and $\alpha_{K^2} = 0.1$ for our bias measurements at $f_{\text{NL}} = 100$.

C Priors and profiles

Figure 10 shows the impact of changing the Poisson noise level (through effective number density in a cell \bar{n}) and of adjusting the prior width on b_ϕ . Here all quadratic bias values are fixed to zero in the mock, but b_δ is set as in Section 4.1 and b_ϕ is set using the UMF relation eqn. 2.3. In this Appendix, we are interested in the impact of priors on statistical constraining power so fix f_{NL} to the true value used in generating the mock (here $f_{\text{NL}} = 7$), but of course a systematic error can bias inferred f_{NL} results. Each color shade corresponds to a different choice of b_1 and b_ϕ values in the perturbative field-level mock. Here we consider a linear model, and what is effectively a linear mock. Moving down a column corresponds to decreasing the injected Poisson noise level, while moving across a row shows the impact of weaker priors. The prior widths considered here, when small, significantly shrink the size of the f_{NL} constraint uncertainties when the injected Poisson noise is larger (lower \bar{n}), though a more modest effect is still visible for lower noise (higher \bar{n}). Clearly, if particularly aggressive yet trusted priors on b_ϕ are available (e.g. from simulations), a concomitant reduction in $\sigma(f_{\text{NL}})$ is possible. However, as we discuss in the main text, the linear model used for the

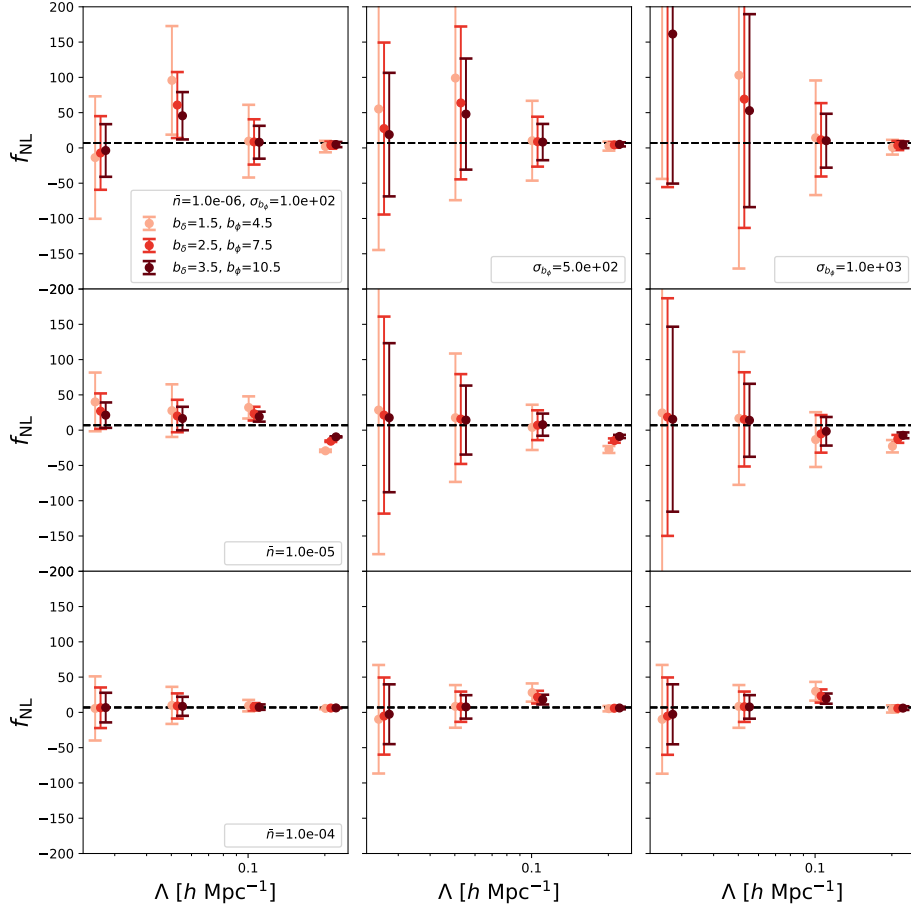


Figure 10. The impact of both prior strength (columns) and number density (rows) on the profile constraints of f_{NL} (similar to Fig. 4, but see the text for differences). Different color shades indicate values of b_δ and b_ϕ used to generate the perturbative field level mock. Rows correspond to different levels of injected Poisson noise corresponding to number densities \bar{n} given in $[h/\text{Mpc}]^3$, while columns correspond to different prior width assumptions for b_ϕ .

illustration in Figure 10 is almost assured to generate statistically biased f_{NL} when applied to realistic tracers.

References

- [1] A. Achúcarro, M. Biagetti, M. Braglia, G. Cabass, R. Caldwell, E. Castorina et al., *Inflation: Theory and Observations*, *arXiv e-prints* (2022) [arXiv:2203.08128](#) [[2203.08128](#)].
- [2] P. D. Meerburg, D. Green, R. Flauger, B. Wallisch, M. C. D. Marsh, E. Pajer et al., *Primordial Non-Gaussianity*, *BAAS* **51** (2019) 107 [[1903.04409](#)].
- [3] E. Komatsu and D. N. Spergel, *Acoustic signatures in the primary microwave background bispectrum*, *Phys. Rev. D* **63** (2001) 063002 [[astro-ph/0005036](#)].
- [4] X. Chen, *Primordial Non-Gaussianities from Inflation Models*, *Advances in Astronomy* **2010** (2010) 638979 [[1002.1416](#)].

- [5] M. Liguori, E. Sefusatti, J. R. Fergusson and E. P. S. Shellard, *Primordial Non-Gaussianity and Bispectrum Measurements in the Cosmic Microwave Background and Large-Scale Structure*, *Advances in Astronomy* **2010** (2010) 980523 [1001.4707].
- [6] P. Creminelli, L. Senatore and M. Zaldarriaga, *Estimators for local non-Gaussianities*, *J. Cosmology Astropart. Phys.* **2007** (2007) 019 [astro-ph/0606001].
- [7] D. Wands, *Local non-Gaussianity from inflation*, *Classical and Quantum Gravity* **27** (2010) 124002 [1004.0818].
- [8] J. Maldacena, *Non-gaussian features of primordial fluctuations in single field inflationary models*, *Journal of High Energy Physics* **2003** (2003) 013 [astro-ph/0210603].
- [9] V. Acquaviva, N. Bartolo, S. Matarrese and A. Riotto, *Gauge-invariant second-order perturbations and non-Gaussianity from inflation*, *Nuclear Physics B* **667** (2003) 119 [astro-ph/0209156].
- [10] E. Pajer, F. Schmidt and M. Zaldarriaga, *The Observed squeezed limit of cosmological three-point functions*, *Phys. Rev. D* **88** (2013) 083502 [1305.0824].
- [11] Planck Collaboration, Y. Akrami, F. Arroja, M. Ashdown, J. Aumont, C. Baccigalupi et al., *Planck 2018 results. IX. Constraints on primordial non-Gaussianity*, *A&A* **641** (2020) A9 [1905.05697].
- [12] J. R. Fergusson and E. P. S. Shellard, *Primordial non-Gaussianity and the CMB bispectrum*, *Phys. Rev. D* **76** (2007) 083523 [astro-ph/0612713].
- [13] O. Doré, J. Bock, M. Ashby, P. Capak, A. Cooray, R. de Putter et al., *Cosmology with the SPHEREX All-Sky Spectral Survey*, *arXiv e-prints* (2014) arXiv:1412.4872 [1412.4872].
- [14] R. de Putter and O. Doré, *Designing an inflation galaxy survey: How to measure $\sigma(f_{NL}) \sim 1$ using scale-dependent galaxy bias*, *Phys. Rev. D* **95** (2017) 123513 [1412.3854].
- [15] C. Heinrich, O. Doré and E. Krause, *Measuring f_{NL} with the SPHEREx multitracer redshift space bispectrum*, *Phys. Rev. D* **109** (2024) 123511 [2311.13082].
- [16] D. Green, Y. Guo, J. Han and B. Wallisch, *Light fields during inflation from BOSS and future galaxy surveys*, *J. Cosmology Astropart. Phys.* **2024** (2024) 090 [2311.04882].
- [17] M. Schmittfull and U. Seljak, *Parameter constraints from cross-correlation of CMB lensing with galaxy clustering*, *Phys. Rev. D* **97** (2018) 123540 [1710.09465].
- [18] J. M. Sullivan, T. Prijon and U. Seljak, *Learning to concentrate: multi-tracer forecasts on local primordial non-Gaussianity with machine-learned bias*, *J. Cosmology Astropart. Phys.* **2023** (2023) 004 [2303.08901].
- [19] E. Castorina, Y. Feng, U. Seljak and F. Villaescusa-Navarro, *Primordial Non-Gaussianities and Zero-Bias Tracers of the Large-Scale Structure*, *Phys. Rev. Lett.* **121** (2018) 101301 [1803.11539].
- [20] U. Seljak, *Extracting Primordial Non-Gaussianity without Cosmic Variance*, *Phys. Rev. Lett.* **102** (2009) 021302 [0807.1770].
- [21] M. Alvarez, T. Baldauf, J. R. Bond, N. Dalal, R. de Putter, O. Doré et al., *Testing Inflation with Large Scale Structure: Connecting Hopes with Reality*, *arXiv e-prints* (2014) arXiv:1412.4671 [1412.4671].
- [22] A. Barreira and E. Krause, *Towards optimal and robust f_{NL} constraints with multi-tracer analyses*, *J. Cosmology Astropart. Phys.* **2023** (2023) 044 [2302.09066].
- [23] N. Hamaus, U. Seljak and V. Desjacques, *Optimal constraints on local primordial non-Gaussianity from the two-point statistics of large-scale structure*, *Phys. Rev. D* **84** (2011) 083509 [1104.2321].

- [24] T. Giannantonio, C. Porciani, J. Carron, A. Amara and A. Pillepich, *Constraining primordial non-Gaussianity with future galaxy surveys*, *MNRAS* **422** (2012) 2854 [[1109.0958](#)].
- [25] C. Carbone, L. Verde and S. Matarrese, *Non-Gaussian Halo Bias and Future Galaxy Surveys*, *ApJ* **684** (2008) L1 [[0806.1950](#)].
- [26] D. Alonso, P. Bull, P. G. Ferreira, R. Maartens and M. G. Santos, *Ultra-large-scale Cosmology in Next-generation Experiments with Single Tracers*, *ApJ* **814** (2015) 145 [[1505.07596](#)].
- [27] D. Karagiannis, A. Lazanu, M. Liguori, A. Raccanelli, N. Bartolo and L. Verde, *Constraining primordial non-Gaussianity with bispectrum and power spectrum from upcoming optical and radio surveys*, *MNRAS* **478** (2018) 1341 [[1801.09280](#)].
- [28] A. Moradinezhad Dizgah and G. K. Keating, *Line Intensity Mapping with [C II] and CO(1-0) as Probes of Primordial Non-Gaussianity*, *ApJ* **872** (2019) 126 [[1810.02850](#)].
- [29] T. Flöss, M. Biagetti and P. D. Meerburg, *Primordial non-Gaussianity and non-Gaussian covariance*, *Phys. Rev. D* **107** (2023) 023528 [[2206.10458](#)].
- [30] E. Fondi, L. Verde, F. Villaescusa-Navarro, M. Baldi, W. R. Coulton, G. Jung et al., *Taming assembly bias for primordial non-Gaussianity*, *J. Cosmology Astropart. Phys.* **2024** (2024) 048 [[2311.10088](#)].
- [31] A. Moradinezhad Dizgah, M. Biagetti, E. Sefusatti, V. Desjacques and J. Noreña, *Primordial non-Gaussianity from biased tracers: likelihood analysis of real-space power spectrum and bispectrum*, *J. Cosmology Astropart. Phys.* **2021** (2021) 015 [[2010.14523](#)].
- [32] Z. Brown, R. Demina, A. G. Adame, S. Avila, E. Chaussidon, S. Yuan et al., *Constraining primordial non-Gaussianity from the large scale structure two-point and three-point correlation functions*, *arXiv e-prints* (2024) [arXiv:2403.18789](#) [[2403.18789](#)].
- [33] G. Cabass, M. M. Ivanov, O. H. E. Philcox, M. Simonović and M. Zaldarriaga, *Constraints on multifield inflation from the BOSS galaxy survey*, *Phys. Rev. D* **106** (2022) 043506 [[2204.01781](#)].
- [34] G. D’Amico, M. Lewandowski, L. Senatore and P. Zhang, *Limits on primordial non-Gaussianities from BOSS galaxy-clustering data*, *arXiv e-prints* (2022) [arXiv:2201.11518](#) [[2201.11518](#)].
- [35] N. Dalal, O. Doré, D. Huterer and A. Shirokov, *Imprints of primordial non-Gaussianities on large-scale structure: Scale-dependent bias and abundance of virialized objects*, *Phys. Rev. D* **77** (2008) 123514 [[0710.4560](#)].
- [36] V. Desjacques and U. Seljak, *Primordial non-Gaussianity from the large-scale structure*, *Classical and Quantum Gravity* **27** (2010) 124011 [[1003.5020](#)].
- [37] V. Desjacques, D. Jeong and F. Schmidt, *Large-scale galaxy bias*, *Phys. Rep.* **733** (2018) 1 [[1611.09787](#)].
- [38] V. Assassi, D. Baumann and F. Schmidt, *Galaxy bias and primordial non-Gaussianity*, *J. Cosmology Astropart. Phys.* **2015** (2015) 043 [[1510.03723](#)].
- [39] T. Baldauf, U. Seljak, L. Senatore and M. Zaldarriaga, *Galaxy bias and non-linear structure formation in general relativity*, *J. Cosmology Astropart. Phys.* **2011** (2011) 031 [[1106.5507](#)].
- [40] L. Lucie-Smith, A. Barreira and F. Schmidt, *Halo assembly bias from a deep learning model of halo formation*, *MNRAS* **524** (2023) 1746 [[2304.09880](#)].
- [41] T. Lazeyras, A. Barreira, F. Schmidt and V. Desjacques, *Assembly bias in the local PNG halo bias and its implication for f_{NL} constraints*, *arXiv e-prints* (2022) [arXiv:2209.07251](#) [[2209.07251](#)].
- [42] S. Matarrese and L. Verde, *The Effect of Primordial Non-Gaussianity on Halo Bias*, *ApJ* **677** (2008) L77 [[0801.4826](#)].

- [43] E. Sefusatti and E. Komatsu, *Bispectrum of galaxies from high-redshift galaxy surveys: Primordial non-Gaussianity and nonlinear galaxy bias*, *Phys. Rev. D* **76** (2007) 083004 [0705.0343].
- [44] A. Pillepich, C. Porciani and O. Hahn, *Halo mass function and scale-dependent bias from N -body simulations with non-Gaussian initial conditions*, *MNRAS* **402** (2010) 191 [0811.4176].
- [45] V. Desjacques, U. Seljak and I. T. Iliev, *Scale-dependent bias induced by local non-Gaussianity: a comparison to N -body simulations*, *MNRAS* **396** (2009) 85 [0811.2748].
- [46] N. Afshordi and A. J. Tolley, *Primordial non-Gaussianity, statistics of collapsed objects, and the integrated Sachs-Wolfe effect*, *Phys. Rev. D* **78** (2008) 123507 [0806.1046].
- [47] R. Scoccimarro, E. Sefusatti and M. Zaldarriaga, *Probing primordial non-Gaussianity with large-scale structure*, *Phys. Rev. D* **69** (2004) 103513 [astro-ph/0312286].
- [48] M. Grossi, L. Verde, C. Carbone, K. Dolag, E. Branchini, F. Iannuzzi et al., *Large-scale non-Gaussian mass function and halo bias: tests on N -body simulations*, *MNRAS* **398** (2009) 321 [0902.2013].
- [49] D. Jeong and E. Komatsu, *Primordial Non-Gaussianity, Scale-dependent Bias, and the Bispectrum of Galaxies*, *ApJ* **703** (2009) 1230 [0904.0497].
- [50] P. McDonald, *Primordial non-Gaussianity: Large-scale structure signature in the perturbative bias model*, *Phys. Rev. D* **78** (2008) 123519 [0806.1061].
- [51] T. Giannantonio and C. Porciani, *Structure formation from non-Gaussian initial conditions: Multivariate biasing, statistics, and comparison with N -body simulations*, *Phys. Rev. D* **81** (2010) 063530 [0911.0017].
- [52] L. Verde and S. Matarrese, *Detectability of the Effect of Inflationary Non-Gaussianity on Halo Bias*, *ApJ* **706** (2009) L91 [0909.3224].
- [53] F. Schmidt and M. Kamionkowski, *Halo clustering with nonlocal non-Gaussianity*, *Phys. Rev. D* **82** (2010) 103002 [1008.0638].
- [54] V. Desjacques, D. Jeong and F. Schmidt, *Non-Gaussian Halo Bias Re-examined: Mass-dependent Amplitude from the Peak-Background Split and Thresholding*, *Phys. Rev. D* **84** (2011) 063512 [1105.3628].
- [55] K. M. Smith, S. Ferraro and M. LoVerde, *Halo clustering and g_{NL} -type primordial non-gaussianity*, *J. Cosmology Astropart. Phys.* **2012** (2012) 032 [1106.0503].
- [56] W. R. Coulton, F. Villaescusa-Navarro, D. Jamieson, M. Baldi, G. Jung, D. Karagiannis et al., *Quijote-PNG: The Information Content of the Halo Power Spectrum and Bispectrum*, *ApJ* **943** (2023) 178 [2206.15450].
- [57] A. Barreira, *The local PNG bias of neutral Hydrogen, H_I* , *J. Cosmology Astropart. Phys.* **2022** (2022) 057 [2112.03253].
- [58] P. McDonald, *Primordial non-Gaussianity: Large-scale structure signature in the perturbative bias model*, *Phys. Rev. D* **78** (2008) 123519 [0806.1061].
- [59] A. G. Adame, S. Avila, V. Gonzalez-Perez, G. Yepes, M. Pellejero, M. S. Wang et al., *PNG-UNITsims: Halo clustering response to primordial non-Gaussianities as a function of mass*, *arXiv e-prints* (2023) arXiv:2312.12405 [2312.12405].
- [60] B. Hadzhiyska, L. H. Garrison, D. J. Eisenstein and S. Ferraro, *Modest set of simulations of local-type primordial non-Gaussianity in the DESI era*, *Phys. Rev. D* **109** (2024) 103530 [2402.10881].

- [61] T. Lazeyras, A. Barreira and F. Schmidt, *Assembly bias in quadratic bias parameters of dark matter halos from forward modeling*, *J. Cosmology Astropart. Phys.* **2021** (2021) 063 [[2106.14713](#)].
- [62] E.-M. Mueller, M. Rezaie, W. J. Percival, A. J. Ross, R. Ruggeri, H.-J. Seo et al., *The clustering of galaxies in the completed SDSS-IV extended Baryon Oscillation Spectroscopic Survey: Primordial non-Gaussianity in Fourier Space*, *arXiv e-prints* (2021) arXiv:2106.13725 [[2106.13725](#)].
- [63] M. Rezaie, A. J. Ross, H.-J. Seo, H. Kong, A. Porredon, L. Samushia et al., *Local primordial non-Gaussianity from the large-scale clustering of photometric DESI luminous red galaxies*, *MNRAS* (2024) [[2307.01753](#)].
- [64] E. Castorina, N. Hand, U. Seljak, F. Beutler, C.-H. Chuang, C. Zhao et al., *Redshift-weighted constraints on primordial non-Gaussianity from the clustering of the eBOSS DR14 quasars in Fourier space*, *J. Cosmology Astropart. Phys.* **2019** (2019) 010 [[1904.08859](#)].
- [65] A. Slosar, C. Hirata, U. Seljak, S. Ho and N. Padmanabhan, *Constraints on local primordial non-Gaussianity from large scale structure*, *J. Cosmology Astropart. Phys.* **2008** (2008) 031 [[0805.3580](#)].
- [66] B. Leistedt, H. V. Peiris and N. Roth, *Constraints on Primordial Non-Gaussianity from 800 000 Photometric Quasars*, *Phys. Rev. Lett.* **113** (2014) 221301 [[1405.4315](#)].
- [67] A. Barreira, *Can we actually constrain f_{NL} using the scale-dependent bias effect? An illustration of the impact of galaxy bias uncertainties using the BOSS DR12 galaxy power spectrum*, *J. Cosmology Astropart. Phys.* **2022** (2022) 013 [[2205.05673](#)].
- [68] M. S. Cagliari, E. Castorina, M. Bonici and D. Bianchi, *Optimal constraints on Primordial non-Gaussianity with the eBOSS DR16 quasars in Fourier space*, *arXiv e-prints* (2023) arXiv:2309.15814 [[2309.15814](#)].
- [69] F. McCarthy, M. S. Madhavacheril and A. S. Maniyar, *Constraints on primordial non-Gaussianity from halo bias measured through CMB lensing cross-correlations*, *Phys. Rev. D* **108** (2023) 083522 [[2210.01049](#)].
- [70] A. Barreira, *On the impact of galaxy bias uncertainties on primordial non-Gaussianity constraints*, *J. Cosmology Astropart. Phys.* **2020** (2020) 031 [[2009.06622](#)].
- [71] A. Barreira, G. Cabass, F. Schmidt, A. Pillepich and D. Nelson, *Galaxy bias and primordial non-Gaussianity: insights from galaxy formation simulations with IllustrisTNG*, *J. Cosmology Astropart. Phys.* **2020** (2020) 013 [[2006.09368](#)].
- [72] B. A. Reid, L. Verde, K. Dolag, S. Matarrese and L. Moscardini, *Non-Gaussian halo assembly bias*, *J. Cosmology Astropart. Phys.* **2010** (2010) 013 [[1004.1637](#)].
- [73] J. M. Sullivan, U. Seljak and S. Singh, *An analytic hybrid halo + perturbation theory model for small-scale correlators: baryons, halos, and galaxies*, *J. Cosmology Astropart. Phys.* **2021** (2021) 026 [[2104.10676](#)].
- [74] M. M. Ivanov, C. Cuesta-Lazaro, S. Mishra-Sharma, A. Obuljen and M. W. Toomey, *Full-shape analysis with simulation-based priors: constraints on single field inflation from BOSS*, *arXiv e-prints* (2024) arXiv:2402.13310 [[2402.13310](#)].
- [75] M. Peron, G. Jung, M. Liguori and M. Pietroni, *Constraining Primordial Non-Gaussianity from Large Scale Structure with the Wavelet Scattering Transform*, *arXiv e-prints* (2024) arXiv:2403.17657 [[2403.17657](#)].
- [76] W. R. Coulton, T. Abel and A. Banerjee, *Small-scale signatures of primordial non-Gaussianity in k -Nearest Neighbour cumulative distribution functions*, *arXiv e-prints* (2023) arXiv:2309.15151 [[2309.15151](#)].

- [77] G. Jung, A. Ravenni, M. Liguori, M. Baldi, W. R. Coulton, F. Villaescusa-Navarro et al., *Quijote-PNG: Optimizing the summary statistics to measure Primordial non-Gaussianity*, *arXiv e-prints* (2024) arXiv:2403.00490 [2403.00490].
- [78] G. Jung, A. Ravenni, M. Baldi, W. R. Coulton, D. Jamieson, D. Karagiannis et al., *Quijote-PNG: The Information Content of the Halo Mass Function*, *ApJ* **957** (2023) 50 [2305.10597].
- [79] J. H. T. Yip, M. Biagetti, A. Cole, K. Viswanathan and G. Shiu, *Cosmology with Persistent Homology: a Fisher Forecast*, *arXiv e-prints* (2024) arXiv:2403.13985 [2403.13985].
- [80] M. Biagetti, J. Calles, L. Castiblanco, A. Cole and J. Noreña, *Fisher forecasts for primordial non-Gaussianity from persistent homology*, *J. Cosmology Astropart. Phys.* **2022** (2022) 002 [2203.08262].
- [81] D. Jamieson, Y. Li, R. A. de Oliveira, F. Villaescusa-Navarro, S. Ho and D. N. Spergel, *Field-level Neural Network Emulator for Cosmological N-body Simulations*, *ApJ* **952** (2023) 145 [2206.04594].
- [82] M. Schmittfull, M. Simonović, V. Assassi and M. Zaldarriaga, *Modeling biased tracers at the field level*, *Phys. Rev. D* **100** (2019) 043514 [1811.10640].
- [83] M. Schmittfull, M. Simonović, M. M. Ivanov, O. H. E. Philcox and M. Zaldarriaga, *Modeling galaxies in redshift space at the field level*, *J. Cosmology Astropart. Phys.* **2021** (2021) 059 [2012.03334].
- [84] N.-M. Nguyen, F. Schmidt, B. Tucci, M. Reinecke and A. Kostić, *How much information can be extracted from galaxy clustering at the field level?*, *arXiv e-prints* (2024) arXiv:2403.03220 [2403.03220].
- [85] F. Elsner, F. Schmidt, J. Jasche, G. Lavaux and N.-M. Nguyen, *Cosmology inference from a biased density field using the EFT-based likelihood*, *J. Cosmology Astropart. Phys.* **2020** (2020) 029 [1906.07143].
- [86] F. Schmidt, F. Elsner, J. Jasche, N. M. Nguyen and G. Lavaux, *A rigorous EFT-based forward model for large-scale structure*, *J. Cosmology Astropart. Phys.* **2019** (2019) 042 [1808.02002].
- [87] F. Schmidt, G. Cabass, J. Jasche and G. Lavaux, *Unbiased cosmology inference from biased tracers using the EFT likelihood*, *J. Cosmology Astropart. Phys.* **2020** (2020) 008 [2004.06707].
- [88] F. Schmidt, *Sigma-eight at the percent level: the EFT likelihood in real space*, *J. Cosmology Astropart. Phys.* **2021** (2021) 032 [2009.14176].
- [89] J. Stadler, F. Schmidt and M. Reinecke, *Cosmology inference at the field level from biased tracers in redshift-space*, *arXiv e-prints* (2023) arXiv:2303.09876 [2303.09876].
- [90] A. Kostić, N.-M. Nguyen, F. Schmidt and M. Reinecke, *Consistency tests of field level inference with the EFT likelihood*, *arXiv e-prints* (2022) arXiv:2212.07875 [2212.07875].
- [91] A. Obuljen, M. Simonović, A. Schneider and R. Feldmann, *Modeling HI at the field level*, *arXiv e-prints* (2022) arXiv:2207.12398 [2207.12398].
- [92] G. Cabass, M. Simonović and M. Zaldarriaga, *Cosmological Information in Perturbative Forward Modeling*, *arXiv e-prints* (2023) arXiv:2307.04706 [2307.04706].
- [93] D. Baumann and D. Green, *The power of locality: primordial non-Gaussianity at the map level*, *J. Cosmology Astropart. Phys.* **2022** (2022) 061 [2112.14645].
- [94] S. Ferraro and K. M. Smith, *Using large scale structure to measure f_{NL} , g_{NL} and τ_{NL}* , *Phys. Rev. D* **91** (2015) 043506 [1408.3126].

- [95] T. Baldauf, U. Seljak, L. Senatore and M. Zaldarriaga, *Linear response to long wavelength fluctuations using curvature simulations*, *J. Cosmology Astropart. Phys.* **2016** (2016) 007 [[1511.01465](#)].
- [96] T. Matsubara, *Nonlinear perturbation theory with halo bias and redshift-space distortions via the Lagrangian picture*, *Phys. Rev. D* **78** (2008) 083519 [[0807.1733](#)].
- [97] Z. Vlah, E. Castorina and M. White, *The Gaussian streaming model and convolution Lagrangian effective field theory*, *J. Cosmology Astropart. Phys.* **2016** (2016) 007 [[1609.02908](#)].
- [98] M. M. Abidi and T. Baldauf, *Cubic halo bias in Eulerian and Lagrangian space*, *J. Cosmology Astropart. Phys.* **2018** (2018) 029 [[1802.07622](#)].
- [99] C. Modi, M. White, A. Slosar and E. Castorina, *Reconstructing large-scale structure with neutral hydrogen surveys*, *J. Cosmology Astropart. Phys.* **2019** (2019) 023 [[1907.02330](#)].
- [100] C. Modi, S.-F. Chen and M. White, *Simulations and symmetries*, *MNRAS* **492** (2020) 5754 [[1910.07097](#)].
- [101] N. Kokron, J. DeRose, S.-F. Chen, M. White and R. H. Wechsler, *Priors on red galaxy stochasticity from hybrid effective field theory*, *MNRAS* **514** (2022) 2198 [[2112.00012](#)].
- [102] M. Pellejero Ibañez, R. E. Angulo, D. Jamieson and Y. Li, *Hybrid bias and displacement emulators for field-level modelling of galaxy clustering in real and redshift space*, *MNRAS* **529** (2024) 89 [[2307.09134](#)].
- [103] M. Pellejero Ibañez, J. Stücker, R. E. Angulo, M. Zennaro, S. Contreras and G. Aricò, *Modelling galaxy clustering in redshift space with a Lagrangian bias formalism and N-body simulations*, *MNRAS* **514** (2022) 3993 [[2109.08699](#)].
- [104] B. Hadzhiyska, C. García-García, D. Alonso, A. Nicola and A. Slosar, *Hefty enhancement of cosmological constraints from the DES Y1 data using a hybrid effective field theory approach to galaxy bias*, *J. Cosmology Astropart. Phys.* **2021** (2021) 020 [[2103.09820](#)].
- [105] N. Kokron, J. DeRose, S.-F. Chen, M. White and R. H. Wechsler, *The cosmology dependence of galaxy clustering and lensing from a hybrid N-body-perturbation theory model*, *MNRAS* **505** (2021) 1422 [[2101.11014](#)].
- [106] D. Baradaran, B. Hadzhiyska, M. J. White and N. Sailer, *Predicting the 21 cm field with a Hybrid Effective Field Theory approach*, *arXiv e-prints* (2024) arXiv:2406.13079 [[2406.13079](#)].
- [107] M. Pellejero Ibañez, R. E. Angulo and J. A. Peacock, *Cosmological constraints from the full-shape galaxy power spectrum in SDSS-III BOSS using the BACCO hybrid Lagrangian bias emulator*, *arXiv e-prints* (2024) arXiv:2407.07949 [[2407.07949](#)].
- [108] F. Maion, R. E. Angulo, T. Bakx, N. E. Chisari, T. Kurita and M. Pellejero-Ibañez, *HYMALAIA: a hybrid lagrangian model for intrinsic alignments*, *MNRAS* **531** (2024) 2684 [[2307.13754](#)].
- [109] G. Cabass and F. Schmidt, *The likelihood for LSS: stochasticity of bias coefficients at all orders*, *J. Cosmology Astropart. Phys.* **2020** (2020) 051 [[2004.00617](#)].
- [110] Y. Feng, M.-Y. Chu, U. Seljak and P. McDonald, *FASTPM: a new scheme for fast simulations of dark matter and haloes*, *MNRAS* **463** (2016) 2273 [[1603.00476](#)].
- [111] A. Lewis, A. Challinor and A. Lasenby, *Efficient Computation of Cosmic Microwave Background Anisotropies in Closed Friedmann-Robertson-Walker Models*, *ApJ* **538** (2000) 473 [[astro-ph/9911177](#)].
- [112] N. Hand, Y. Feng, F. Beutler, Y. Li, C. Modi, U. Seljak et al., *nbodykit: An Open-source, Massively Parallel Toolkit for Large-scale Structure*, *AJ* **156** (2018) 160 [[1712.05834](#)].

- [113] Y. P. Jing, *Correcting for the Alias Effect When Measuring the Power Spectrum Using a Fast Fourier Transform*, *ApJ* **620** (2005) 559 [[astro-ph/0409240](#)].
- [114] A. E. Bayer, U. Seljak and C. Modi, *Field-Level Inference with Microcanonical Langevin Monte Carlo*, *arXiv e-prints* (2023) [arXiv:2307.09504](#) [[2307.09504](#)].
- [115] A. E. Bayer, C. Modi and S. Ferraro, *Joint velocity and density reconstruction of the Universe with nonlinear differentiable forward modeling*, *J. Cosmology Astropart. Phys.* **2023** (2023) 046 [[2210.15649](#)].
- [116] M. Millea and U. Seljak, *Marginal unbiased score expansion and application to CMB lensing*, *Phys. Rev. D* **105** (2022) 103531 [[2112.09354](#)].
- [117] U. Seljak, G. Aslanyan, Y. Feng and C. Modi, *Towards optimal extraction of cosmological information from nonlinear data*, *J. Cosmology Astropart. Phys.* **2017** (2017) 009 [[1706.06645](#)].
- [118] Y. Li, L. Lu, C. Modi, D. Jamieson, Y. Zhang, Y. Feng et al., *pmwd: A Differentiable Cosmological Particle-Mesh N-body Library*, *arXiv e-prints* (2022) [arXiv:2211.09958](#) [[2211.09958](#)].
- [119] B. Dai and U. Seljak, *Multiscale Flow for Robust and Optimal Cosmological Analysis*, *arXiv e-prints* (2023) [arXiv:2306.04689](#) [[2306.04689](#)].
- [120] Y. Feng, U. Seljak and M. Zaldarriaga, *Exploring the posterior surface of the large scale structure reconstruction*, *J. Cosmology Astropart. Phys.* **2018** (2018) 043 [[1804.09687](#)].
- [121] J. Jasche and B. D. Wandelt, *Bayesian physical reconstruction of initial conditions from large-scale structure surveys*, *MNRAS* **432** (2013) 894 [[1203.3639](#)].
- [122] X. Chen, F. Zhu, S. Gaines and N. Padmanabhan, *Effective cosmic density field reconstruction with convolutional neural network*, *MNRAS* **523** (2023) 6272 [[2306.10538](#)].
- [123] X. Chen, N. Padmanabhan and D. J. Eisenstein, *Probing primordial non-Gaussianity by reconstructing the initial conditions*, *arXiv e-prints* (2024) [arXiv:2412.00968](#) [[2412.00968](#)].
- [124] G. Cabass, M. Simonović and M. Zaldarriaga, *Cosmological information in perturbative forward modeling*, *Phys. Rev. D* **109** (2024) 043526 [[2307.04706](#)].
- [125] C. Modi and O. H. E. Philcox, *Hybrid SBI or How I Learned to Stop Worrying and Learn the Likelihood*, *arXiv e-prints* (2023) [arXiv:2309.10270](#) [[2309.10270](#)].
- [126] P. Lemos, L. H. Parker, C. Hahn, S. Ho, M. Eickenberg, J. Hou et al., *SimBIG: Field-level Simulation-based Inference of Large-scale Structure*, in *Machine Learning for Astrophysics*, p. 18, July, 2023, DOI [[2310.15256](#)].
- [127] D. K. Ramanah, G. Lavaux, J. Jasche and B. D. Wandelt, *Cosmological inference from Bayesian forward modelling of deep galaxy redshift surveys*, *A&A* **621** (2019) A69 [[1808.07496](#)].
- [128] T. Flöss and P. D. Meerburg, *Improving constraints on primordial non-Gaussianity using neural network based reconstruction*, *J. Cosmology Astropart. Phys.* **2024** (2024) 031 [[2305.07018](#)].
- [129] D. Jamieson, Y. Li, F. Villaescusa-Navarro, S. Ho and D. N. Spergel, *Field-level Emulation of Cosmic Structure Formation with Cosmology and Redshift Dependence*, *arXiv e-prints* (2024) [arXiv:2408.07699](#) [[2408.07699](#)].
- [130] A. Barreira, *Predictions for local PNG bias in the galaxy power spectrum and bispectrum and the consequences for f_{NL} constraints*, *J. Cosmology Astropart. Phys.* **2022** (2022) 033 [[2107.06887](#)].

- [131] W. R. Coulton, F. Villaescusa-Navarro, D. Jamieson, M. Baldi, G. Jung, D. Karagiannis et al., *Quijote-PNG: Simulations of Primordial Non-Gaussianity and the Information Content of the Matter Field Power Spectrum and Bispectrum*, *ApJ* **943** (2023) 64 [2206.01619].
- [132] G. Jung, D. Karagiannis, M. Liguori, M. Baldi, W. R. Coulton, D. Jamieson et al., *Quijote-PNG: Quasi-maximum Likelihood Estimation of Primordial Non-Gaussianity in the Nonlinear Halo Density Field*, *ApJ* **948** (2023) 135 [2211.07565].
- [133] A. Andrews, J. Jasche, G. Lavaux and F. Schmidt, *Bayesian field-level inference of primordial non-Gaussianity using next-generation galaxy surveys*, *MNRAS* **520** (2023) 5746 [2203.08838].
- [134] J. Stadler, F. Schmidt and M. Reinecke, *Fast, Accurate and Perturbative Forward Modeling of Galaxy Clustering Part I: Galaxies in the Restframe*, *arXiv e-prints* (2024) arXiv:2409.10937 [2409.10937].
- [135] M. M. Ivanov, A. Obuljen, C. Cuesta-Lazaro and M. W. Toomey, *Full-shape analysis with simulation-based priors: cosmological parameters and the structure growth anomaly*, *arXiv e-prints* (2024) arXiv:2409.10609 [2409.10609].
- [136] H. Zhang, M. Bonici, G. D’Amico, S. Paradiso and W. J. Percival, *HOD-informed prior for EFT-based full-shape analyses of LSS*, *arXiv e-prints* (2024) arXiv:2409.12937 [2409.12937].
- [137] D. Karagiannis, R. Maartens, J. Fonseca, S. Camera and C. Clarkson, *Multi-tracer power spectra and bispectra: formalism*, *J. Cosmology Astropart. Phys.* **2024** (2024) 034 [2305.04028].
- [138] D. Ginzburg and V. Desjacques, *Shot noise in multitracer constraints on f_{NL} and relativistic projections: Power spectrum*, *MNRAS* **495** (2020) 932 [1911.11701].
- [139] V. Springel, *The cosmological simulation code GADGET-2*, *MNRAS* **364** (2005) 1105 [astro-ph/0505010].
- [140] F. Schmidt, D. Jeong and V. Desjacques, *Peak-background split, renormalization, and galaxy clustering*, *Phys. Rev. D* **88** (2013) 023515 [1212.0868].
- [141] J. Nocedal and S. J. Wright, *Numerical Optimization*. Springer, New York, NY, USA, 2e ed., 2006.
- [142] P. Virtanen, R. Gommers, T. E. Oliphant, M. Haberland, T. Reddy, D. Cournapeau et al., *SciPy 1.0: fundamental algorithms for scientific computing in Python*, *Nature Methods* **17** (2020) 261 [1907.10121].